Nonlinear optical response of noble gases via the metastable electronic state approach

A. Bahl, E. M. Wright, and M. Kolesik
College of Optical Sciences, University of Arizona, Tucson, Arizona 85721, USA
(Received 1 June 2016; published 29 August 2016)

The goal of this paper is to elucidate the theoretical underpinnings of the metastable electronic state approach (MESA) and demonstrate its utility for the evaluation of the nonlinear optical response of noble-gas atoms with emphasis on the application of the method to the propagation of multicolor optical fields in large-scale, spatially resolved simulations. More specifically, single-active-electron models of various atoms are employed to calculate their nonlinear properties both within the adiabatic approximation, involving a single metastable state and beyond, capturing inertial effects, and wavelength-dependent ionization. Simulations for excitation pulses at different center wavelengths as well as ionization in two-color pulses are presented and compared with numerical solutions of the time-dependent Schrödinger equation. Illustrative examples of the numerical simulation of high-power pulse propagation incorporating MESA data are also presented and showcase the successful application to optical filamentation in the midinfrared region.

DOI: 10.1103/PhysRevA.94.023850

I. INTRODUCTION

As the field of nonlinear optics continues to explore ever deeper into extreme optical pulse propagation regimes, there arises the computational challenge of dealing with ever-increasing high intensities and complex waveforms with concomitant ultrabroadband spectra. In tandem, as the optical waveforms become more complex there is the need to improve the material modeling to properly reflect the salient physics of the light-matter interaction on the time and space scales being probed. Furthermore, for large-scale nonlinear propagation simulations with full spatial and temporal resolution, the challenge is to find computationally economic material models that are microscopically founded, accurate, and do not compromise the underlying physics involved. A number of approaches have been proposed, including the first-principle integration of the Maxwell and Schrödinger equations into a single simulated system [1,2], Kramers–Henneberger atoms [3], and Freeman resonances [4] to name a few. We have advanced the metastable electronic state approach (MESA) [5] for which preliminary results have been very promising in terms of both accuracy and computational economy for several model systems [6,7].

The metastable states that are at the center of the approach discussed in this paper are the Stark resonances in a homogeneous external field that tend to the zero-field bound states. The name is meant to suggest that we concentrate on those states that have relatively long lifetimes. Of course, it has been long recognized in many different fields that resonant states are of great utility as a basis for extracting the properties of physical systems and this despite the fact that they are not elements of the Hilbert space assigned to a quantum system. The Stark resonances in particular have been used previously to describe ionization in strong fields, both for atoms and molecules (see e.g., Refs. [8–10]). In MESA, we take this further, recognizing that, among the Stark resonances, the metastable ones can be used to describe the full *nonlinear optical response* due to an applied field, thereby including not only nonlinear ionization losses but also the concomitant nonlinear refraction. Since the long-lived resonances are slaved to the time-dependent external field, one can extract the *transient* nonlinear optical response as required in the area of ultrafast nonlinear optics. For such applications, the importance of Stark resonances lies in that they uniquely capture the behavior of the system in the no-man's land where neither bound nor free electronic states dominate the nonlinear optical response, and that they enable a *practically useful* method that is computationally effective enough that it can be coupled to large-scale, spatially resolved simulations bridging scales from quantum to macroscopic.

The overall goal of the present paper is to elucidate the theoretical underpinnings of MESA and demonstrate its utility for the evaluation of the nonlinear optical response of noble-gas atoms, with emphasis on the application of the method to nonlinear pulse propagation in large-scale, spatially resolved simulations. MESA stems from the concept of using the metastable states of the atom in the presence of the instantaneous applied electric field as a basis for the portion of the electron wave function that remains correlated with the parent ion: The quasistatic assumption is appropriate here as we are concerned with the off-resonant case in which the photon energies are well removed from the ionization energy. Indeed, using only a single metastable state, this approach already predicts the nonlinear Kerr coefficient of several noble-gas atoms within 20%–50% accuracy [6]: This indicates that in comparison with the conventional unperturbed electronic states, the metastable states "encode" a lot of useful physical information. Ultimately the goal is to compare the predictions from MESA against experiment, but for the present paper we employ numerical solutions of the time-dependent Schrödinger equation (TDSE), using the single-active electron potentials alluded to above, as a measurement of the quality of the MESA data.

The purpose of this paper is twofold: First, we provide the interested reader with the background and data that are needed to implement the light-matter interaction models within the single-state MESA framework for a variety of noble-gas atoms (He, Ne, Ar, Kr, Xe); single-state MESA considers only the lowest metastable state that connects to the atomic ground state at zero electric field. In particular, we provide a tabulation of all necessary quantities extracted from the single-active-electron models, and discuss issues relevant for the software implementation. Illustrative simulations demonstrate the utility of the method for modeling optical filamentation.

The second purpose is to develop corrections to the simplest single-state MESA and gauge their effect as a function of wavelength. Under the employment of the quasistatic or adiabatic approximation, single-state MESA yields a nonlinear optical response that depends only on the instantaneous value of the electric field strength $F(t)$, meaning that the nonlinear response is color blind and does not depend on the time history of the electric field. Thus single-state MESA is suitable in the long-wavelength regime, however the post-adiabatic corrections become relevant for shorter wavelengths and introduce an inertial component to the nonlinear response. Here we develop and quantify post-adiabatic corrections that take approximate account of higher-order metastable states and describe a scheme that greatly improves the comparison of the nonlinear optical response obtained from the TDSE solutions, particularly for shorter wavelengths.

The remainder of this paper is organized as follows: We start with a description of the expansion of the electronic wave function in terms of metastable states, also known as Stark resonant states, followed by the adiabatic single-state MESA approximation and then the post-adiabatic corrections. Next we elaborate how to extract the nonlinear polarization and ionization fraction, along with providing the data pertaining to the single-active electron potentials for the various noble-gas atoms. The post-adiabatic corrections are then assessed in terms of the ionized fraction in comparison to the corresponding TDSE solutions for both single- and two-color pulses, and good agreement is found for a range of intensities and wavelengths. To provide a sense of the relevance of the post-adiabatic corrections, we present comparative simulations in which we model femtosecond optical filamentation in several noble gases for near-infrared and midinfrared high-power pulses. We conclude by pointing out new directions suggested by our investigations.

II. STARK RESONANT STATE EXPANSION

For completeness, we begin with a recapitulation of the MESA [5]. Consider a Hamiltonian for a single-active-electron model of an atom exposed to a time-dependent electric field $F(t)$ (optical pulse) polarized along x (in atomic units):

$$H(t) = -\tfrac{1}{2}\Delta + V(\vec{r}\,) - F(t)x. \tag{1}$$

Here we depart from the standard Hermitian quantum mechanics. The spatial axis pointing in the direction of the field is redefined as a contour in the complex plane that follows the real axis in the inner domain, close to the nucleus, and deviates in the upper and lower half planes for positive and negative large x, respectively. This change is a version of the exterior complex scaling (see, e.g., Ref. [11]). It makes the system open, by giving the domain boundaries that absorb the outgoing waves.

Seeking the solution of the Schödinger equation

$$i\,\partial_t \psi(t) = H(t)\psi(t), \tag{2}$$

the wave function is split into two parts, as

$$\psi(t) = \psi_R(t) + \psi_F(t) = \sum_k c_k(t)\psi_k(F(t)) + \psi_F(t), \tag{3}$$

where $\psi_k(F(t))$ is the kth metastable state driven by the external field, so that at all times t it is an eigenvector of the time-dependent Hamiltonian,

$$H(t)\psi_k(F(t)) = E_k(F(t))\psi_k(F(t)). \tag{4}$$

Here $E_k(F(t))$ stands for the complex-valued energy eigenvalue corresponding to ψ_k. Note that imposing the outgoing boundary conditions shifts the eigenvalues into the lower half of the complex plane, where the imaginary parts reflect the lifetimes and can be interpreted as the ionization rates.

In the MESA framework, it is assumed that $\psi_F(t)$ is a strongly delocalized wave function that evolves without much interaction with the parent ion, while the resonant-state expansion is only used for the portion of the wave function that is a mixture of bound and continuum states that interact with the ion. The coupling between ψ_F and ψ_R is only taken into account indirectly, by assuming that the norm of ψ_F grows as that of ψ_R decays, as has been done in TDSE-based modeling [1]. Akin to the strong-field approximation, ψ_F is treated as subject to only the external field. To calculate the induced current it is therefore sufficient to know the norm $\|\psi_F\|^2$. In such an approximation it is only needed to determine the metastable-state expansion coefficients $c_k(t)$ and deduce the norm $\|\psi_F\|^2$ from it.

We assume that before $F(t)$ attains nonzero values the system is in the ground state, and the corresponding resonance state ψ_0 continues to dominate the wave function of the system at later times.

Inserting the resonant-state series into the Schrödinger equation gives

$$\begin{aligned} &i\,\partial_t[c_k(t)\psi_k(F(t))] + i\,\partial_t\psi_F(t) \\ &\quad = i\sum_k [c_k'(t)\psi_k(F(t)) + c_k(t)F'(t)\partial_F\psi_k(F(t))] \\ &\qquad + i\,\partial_t\psi_F(t) \\ &\quad = \sum_k c_k(t)E_k(F(t))\psi_k(F(t)) + H(t)\psi_F(t). \end{aligned} \tag{5}$$

To find the evolution equations for the expansion coefficients, we need to use projection methods to obtain the component corresponding to a single ψ_k.

Since the resonant states are not integrable, the conventional scalar product cannot be used. However, related to the contour C, which defines the exterior complex scaled domain, is a c-product [11,12] defined by the contour integral

$$\langle\psi_i|\psi_j\rangle = \int_C \psi_i(z)\psi_j(z)dz, \tag{6}$$

in which the integration contour follows the real x axis in the vicinity of the atom, and deviates into the upper (lower) complex plane asymptotically for positive (negative) values of x [13]. Metastable states are orthogonal with respect to this c product and are assumed to be orthonormal at all times:

$$\langle\psi_i|\psi_j\rangle = \langle\psi_i|\psi_i\rangle\delta_{ij} = \delta_{ij}. \tag{7}$$

Projecting into the subspace of the nth Stark resonant state $[|\psi_n(F(t))\rangle = |\psi_n\rangle]$ gives the evolution equation

$$\begin{aligned} &i c_n'(t)\langle\psi_n|\psi_n\rangle + i\sum_k c_k(t)F'(t)\langle\psi_n|\partial_F\psi_k(F(t))\rangle \\ &\quad = c_n(t)E_n(F(t))\langle\psi_n|\psi_n\rangle + \langle\psi_n|[H(t) - i\,\partial_t]|\psi_F(t)\rangle. \end{aligned} \tag{8}$$

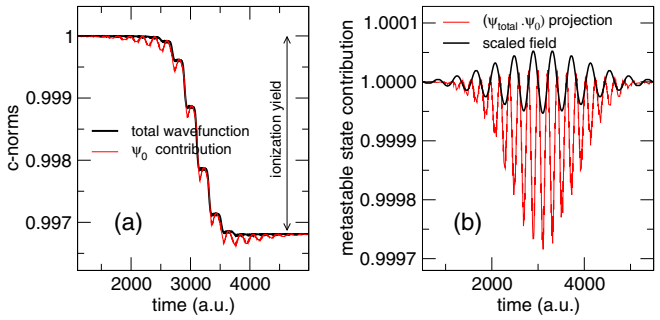

FIG. 1. A TDSE simulation illustrating the dominant contribution of the time-dependent metastable ground state $\psi_0(F(t))$ to the total wave function. Higher-energy resonances show up in the fast but small oscillations in the thin red curve. This simulation (see text for details) was for argon exposed to a 35 fs pulse at 3000 nm wavelength.

The last term represents the coupling to the "freely propagating" component of the wave function, which we neglect on the assumption that the coupling between the different resonant states is more important.

While the above assumption does not hold in general and there is no rigorous criterion to decide when it does, numerical solutions of TDSE indicate that in the specific situations treated here it is a good approximation. Specifically, if the evolution starts in the ground state, and if the ionization remains weak, one can calculate a projection onto a field-dependent resonance state to show that it makes up for nearly all of the total wave function. This makes us confident that, under such conditions, the last term in Eq. (8) can be neglected. Naturally, this assumption can only be tested indirectly with the help of comparison against numerically exact solutions, and this is one of the main points of this work.

Another tacit assumption is about incoming waves which are always present in an expansion into energy eigenstates. Rather then including them explicitly in our expansion, we assume they contribute to ψ_F. Because the latter must be sufficiently delocalized for our approximation to work, we need to require the same from the incoming part of the wave function. Since we never calculate it explicitly, this assumption can only be checked indirectly.

Figure 1 illustrates that the time-dependent (i.e., slaved to the instantaneous field) metastable ground state $\psi_0(F(t))$ dominates the total wave function. Here we have simulated an argon atom exposed to a $\lambda = 3000$ nm, 35 fs pulsed field with a peak amplitude of 0.05 a.u. During the evolution, which started in the ground state, we evaluated the c-norm of the full wave function and the projection of the wave function onto $\psi_0(F(t))$, which is the leading coefficient in the resonant-state expansion, $c_0(t) = \langle\psi_0(F(t))|\psi(t)\rangle$.

The left panel in Fig. 1 shows how the c norm of the full wave function decreases due to ionization. After the excitation pulse abates, the final deviation from unity, indicated by an arrow in the figure, can be interpreted as the ionization yield. Also shown in the same figure is the absolute value of the projection of the total wave function onto ψ_0, i.e., $|c_0(t)| = |\langle\psi_0(F(t))|\psi(t)\rangle|$. It is evident that the full wave function is completely dominated by this metastable state, because the deviations between the two curves are significantly smaller than unity or even the ionization yield.

Panel (b) in Fig. 1 is a visualization of the time-dependent fraction of the metastable state, $|c_0(t)|/||\psi(t)||$, on a finer scale. It shows that more than 99.76% of the total wave function is in fact $\psi_0(F(t))$! Thus, not only the neglected last term in Eq. (8) must be small, but also the rest of the resonant-state expansion is small in comparison with the dominant contribution of the metastable ground state. Observations like these give us confidence that the above assumptions are indeed good approximations, at least in certain regimes.

Returning to our derivations, and adopting these assumptions then yields the following system of ordinary differential equations (ODEs) for the amplitudes $c_n(t)$:

$$c_n'(t) = -ic_n(t)E_n(F(t)) - \sum_k c_k(t)F'(t)\langle\psi_n|\partial_F\psi_k(F(t))\rangle. \tag{9}$$

Retaining a single term in the above amounts to an adiabatic approximation in which the decay of the metastable ground state ψ_0 depends only on the instantaneous value $E_0(F(t))$ [5]. Here the aim is to account for the effects related to the higher-energy Stark resonances in an approximate manner.

A. Post-adiabatic correction of the ionization rate

The temporal evolution of the resonant state amplitudes are controlled by the coupling terms $\langle\psi_n|\partial_F\psi_k(F(t))\rangle$, which can be calculated explicitly in certain exactly solvable models [13]. Such results indicate that the coupling strength increases with the energy; it is therefore not advisable to truncate the above system. Instead, we account for all states ψ_k albeit only approximately.

Integrating the ODE for $c_n(t)$, $n > 0$, one obtains

$$c_n(t) = -\sum_k \int_0^t dt' e^{-iI_n(t',t)}c_k(t')F'(t')U_{nk}(t'), \tag{10}$$

where we introduced the following notation:

$$I_n(t',t) = \int_{t'}^t E_n(F(u))du, \tag{11}$$

$$U_{nk}(t') = \langle\psi_n|\partial_F\psi_k(F(t'))\rangle. \tag{12}$$

For $n > 0$ we will only keep the dominant term that represents the population transfer from the metastable ground state,

$$c_n(t) \approx -\int_0^t dt' e^{-iI_n(t',t)}c_0(t')F'(t')U_{n0}(t'). \tag{13}$$

This approximation is motivated by the fact that the decay of states $\psi_{n>0}$ is much faster than that of $\psi_{k=0}$, and their population is therefore mostly generated from $c_0(t')$. Inserting the approximate expression for $c_n(t)$ into the equation governing $c_0(t)$ we have

$$c_0'(t) = -ic_0(t)E_0(F(t)) + \sum_{n\neq 0}\int_0^t dt' e^{-iI_n(t',t)}c_0(t')F'(t')U_{n0}(t')F'(t)U_{0n}(t). \tag{14}$$

We expect small $t - t' (=\tau)$ to contribute the most to the above integral since $F(t')$ changes slowly on the atomic timescale, so the following approximations can be made:

$$c_0(t') \approx c_0(t)e^{-iI_0(t,t')} = c_0(t)e^{+iI_0(t',t)}, \tag{15}$$

$$U_{n0}(t') = \langle\psi_n|\partial_F\psi_0(F(t'))\rangle \approx U_{n0}(t), \tag{16}$$

$$I_n(t,t') \approx E_n(F(t))(t - t'). \tag{17}$$

Rewriting $c_0(t)$ with these approximations we arrive at

$$c_0'(t) = -iE_R(t)c_0(t), \tag{18}$$

where the correction shows up as a time-dependent, renormalized complex energy of the ground-state resonance,

$$E_R(t) = E_0(F(t)) + iF'(t)\int_0^t dt'F'(t')\mathcal{M}(F(t),t - t'), \tag{19}$$

whose memory kernel is

$$\mathcal{M}(F(t),\tau) = \sum_{n\neq 0} U_{n0}(t)U_{0n}(t)e^{-i[E_n(F(t))-E_0(F(t))]\tau}. \tag{20}$$

This result is still impractical, because it requires the knowledge of the coupling elements U_{n0}, which are difficult to evaluate numerically in realistic models of atoms. Moreover, it is not obvious whether the sum could be meaningfully truncated after a small number of terms.

B. Further memory-function approximations

The next step is to find out more about this memory kernel, beginning with its value at zero delay $\tau = 0$:

$$\begin{aligned}\mathcal{M}(F(t),0) &= \sum_{n\neq 0} U_{n0}(t)U_{0n}(t)\\ &= \sum_{n\neq 0}\langle\psi_n|\partial_F\psi_0(F(t))\rangle\langle\psi_0|\partial_F\psi_n(F(t))\rangle.\end{aligned} \tag{21}$$

Because the c product is symmetric, and the resonant states are normalized to unity at all times, it is such

$$\langle\psi_0|\partial_F\psi_n(F(t))\rangle = -\langle\partial_F\psi_0(F(t))|\psi_n\rangle, \tag{22}$$

and therefore the memory function can be equivalently written as

$$\mathcal{M}(F(t),0) = -\sum_{n\neq 0}\langle\partial_F\psi_0(F(t))|\psi_n\rangle\langle\psi_n|\partial_F\psi_0(F(t))\rangle. \tag{23}$$

At this point we apply a transformation akin to sum rules for dipole moments and reduce the memory function to an expression that only requires the knowledge of the metastable ground state.

To proceed, we need to ask if a wave function evolved from the initial ground state under an excitation with an arbitrary pulse can be decomposed into resonances. This is a question of completeness and, in particular for Stark resonances, it is rather complex and far from fully understood. Rigorous results are rare and only available for a few simple systems, such as Gamow resonances in a compact one-dimensional (1D) potential [14]. For Stark resonances we have recently shown that the resonant state expansion in a 1D system with the Dirac-δ potential is convergent [15], but the series only represents the given function in a half space. Mathematically similar results are available for leaky modes in optical cavities [16,17], where the convergence occurs inside the cavity but not outside. We have recently obtained an exact (as of yet unpublished) result showing the completeness of Stark resonances for a general 1D Hamiltonian with a compact-support potential. The above discussion provides motivation to invoke an "approximate completeness relation" written as

$$1 = |\psi_0\rangle\langle\psi_0| + \sum_{n\neq 0}|\psi_n\rangle\langle\psi_n| + \cdots. \tag{24}$$

Together with the property

$$\langle\partial_F\psi_0|\psi_0\rangle = \langle\psi_0|\partial_F\psi_0\rangle = 0, \tag{25}$$

the elimination of $\sum_{n\neq 0}|\psi_n\rangle\langle\psi_n|$ leads to a reduction solely dependent on the ground-state resonance

$$\mathcal{M}(F,0) = -\langle\partial_F\psi_0(F)|\partial_F\psi_0(F)\rangle. \tag{26}$$

This quantity can be obtained numerically and tabulated for a particular atom. So we have an estimate of the memory function for zero delay. For later times, the memory kernel must be further approximated. We choose to utilize a simple Debye-type functional form parametrized by an effective energy E_{eff}

$$\mathcal{M}(F(t),\tau) = \mathcal{M}(F(t),0)e^{-iE_{\text{eff}}(F(t))\tau}. \tag{27}$$

Thus we arrive at an expression for the time-dependent, renormalized metastable energy, represented as a convolution with the memory kernel that includes nonperturbative dependence on the field intensity but is approximately translation-invariant in time

$$E_R(t) = E_0(F(t)) + iF'(t)\int_0^t dt'F'(t')\mathcal{M}(F(t),0)e^{iE_{\text{eff}}(t'-t)}. \tag{28}$$

$E_{\text{eff}}(t)$ will be most affected by the energy gap between the metastable ground state and higher excited states, causing it to be on the atomic scale and therefore much faster than the field $F(t')$. Calculating the asymptotic contribution to the memory function integral then gives

$$E_R(t) = E_0(F(t)) + \frac{(F'(t))^2}{E_{\text{eff}}(F(t))}\mathcal{M}(F(t),0). \tag{29}$$

This form of the post-adiabatic correction was shown to work reasonably well in simple model systems [5]. However, given the number of approximations adopted in the above derivations, it is necessary to test this result against numerically exact solutions for the same atom models used to obtain all MESA-related characteristics. This is done in the following sections.

III. NONLINEAR POLARIZATION AND IONIZATION

In the approximation outlined in the previous sections, the MESA method requires several quantities to characterize a particular atom. The first is the generalized dipole moment induced by the external field,

$$D(F) = \langle\psi_0(F)|x|\psi_0(F)\rangle, \tag{30}$$

and specifically its nonlinear component with respect to field strength F

$$D_{NL}(F) = D(F) - \lim_{s\to 0} \frac{D(sF)}{s}. \tag{31}$$

Note that the nonlinear dipole moment is a complex-valued quantity, from which MESA utilizes the real part. The imaginary part can be ignored which follows from the formal resonant-state expansion where the imaginary contributions from different expansion components must mutually cancel. (Note that the imaginary part does, however, carry potentially useful information because it is related to the ionization rate.)

The other quantities needed are the imaginary part of the metastable ground-state energy, $E_0(F)$, the post-adiabatic correction $\mathcal{M}(F(t),0)$, and the correction effective parameter E_{eff}, which together govern the temporal evolution of the ionized fraction $\rho(t)$ of atoms through the renormalized $E_R(F)$ as in

$$\partial_t \rho(t) = 2\text{Im}\{E_R(F(t))\}[1-\rho(t)] + \cdots, \tag{32}$$

where the ellipses represent other potential ionization channels such as avalanche and possibly recombination processes. Having calculated the ionized fraction, we use it to evaluate the current induced by the driving field by integrating

$$\partial_t J(t) = e\rho(t)E(t) + \cdots. \tag{33}$$

Above, electron collisions can be included as in the conventional model with the help of an effective damping parameter. The ionized fraction also affects (albeit only weakly) the nonlinear polarization which is obtained as

$$P_{NL}(F) = N_a[1-\rho(t)]D_{NL}(F(t)). \tag{34}$$

The structure of the light-matter interaction model is thus analogous to that of the conventional model used in filamentation, and the two are nearly identical from the standpoint of computational complexity. However, the way the MESA description is parametrized is both more consistent and robust, because it includes interactions between the pure Kerr effect and ensures a proper relative weight between the nonlinear polarization P_{NL} and the defocusing effects of the induced current J.

We have tabulated quantities $D_{NL}(F)$, $E_0(F)$, and $\mathcal{M}(F,0)$ for the single-active-electron (SAE) models of He, Ne, Ar, Kr, and Xe atoms. In these calculations we utilized SAE potentials specified in Refs. [18–20], and used the FEAST eigenvalue solver [21] to obtain the metastable wave functions. To enable interested readers to implement and use the MESA light-matter interaction description in pulse propagation simulation, the Supplemental Material [22] includes these data sets.

The remaining MESA-related characteristics of a given atom model is E_{eff}. Being built upon several approximations, this effective parameter needs to be adjusted and tested with the help of time-domain Schrödinger equation (TDSE) simulations utilizing the same SAE-potentials.

IV. ASSESSMENT OF POST-ADIABATIC CORRECTIONS

The most important manifestation of post-adiabatic corrections in MESA-based models is in the wavelength dependence of the ionization yield from atoms exposed to excitation with different color pulses. The physical mechanism underlying such departures from the adiabatic (or nearly wavelength-independent) behavior is that electronic states with higher energies become heavily damped under the influence of the external field than the ground-state Stark resonance. When the external field changes with time, it introduces a coupling between different resonant states, and this occurs even if field-free selection rules forbid the transitions. This coupling results in the the excitation into higher lying states, and subsequently causes additional ionization. Roughly speaking, higher-energy states open additional ionization channels. This mechanism is closely related to that put forward recently for tunneling from the excited electronic states [23].

A. Ionization in femtosecond pulses

Here we use TDSE simulations with pulsed excitation and compare the simulated ionization fractions to their MESA-based counterparts. To select a value of the parameter E_{eff} for each species, we used the results for longer wavelength, $\lambda = 3\ \mu$m, for which one expects the correction to be relatively small. We adjusted E_{eff} such that the corrected ionization rate is close to but not greater than the numerically measured rate from TDSE. The rationale for not fitting the two sets of results is that we expect the correction to decrease the gap between the model and the numerically exact result but not to capture the deviation in its entirety.

The duration and the intensity of the excitation pulse was chosen to drive the model atoms into a regime typical for optical filamentation, where the ionized fractions range from 10^{-4} to 10^{-2}. The pulse duration was kept as 40 fs, and the intensity was adjusted between different species so that the yield fell into and around this range.

The TDSE simulations were performed on grids 800×400 (along z and radial dimensions, respectively) for He, Ne, Ar, Kr, and Xe. To improve the accuracy while keeping the computational complexity reasonably low, we used inhomogeneous grids with grid spacings ranging from $\sim$0.02 a.u. in the center to about 0.2 a.u. at large distances from it. These calculations utilized the complex-scaled computational domains which act as transparent boundary conditions [24] for outgoing waves and used five-point discretization schemes. This allowed us to use relatively small computational domains, $z \sim 60$ a.u. It is important that the TDSE simulation represents exactly the same open (i.e., norm nonconserving) system as the one used to extract all MESA-related quantities and post-adiabatic corrections. This way we are in the position to study the role of the MESA-related approximations where the TDSE results can be taken as a "numerically exact" target solution.

The results of the MESA-TDSE comparisons are shown in Fig. 2. The solid lines show the uncorrected MESA result which represents the long-wavelength, or adiabatic limit. The other dashed lines are obtained with the inclusion of the post-adiabatic corrections with a fixed parameter E_{eff}, using $E_{\text{eff}} = 0.17,\ 0.14,\ 0.12,\ 0.11,\ 0.10$ for He, Ne, Ar, Kr, and Xe, respectively.

Note that these values are lower than one could expect based on a gap between the ground and excited state(s). This indicates that a physical significance should not be attached

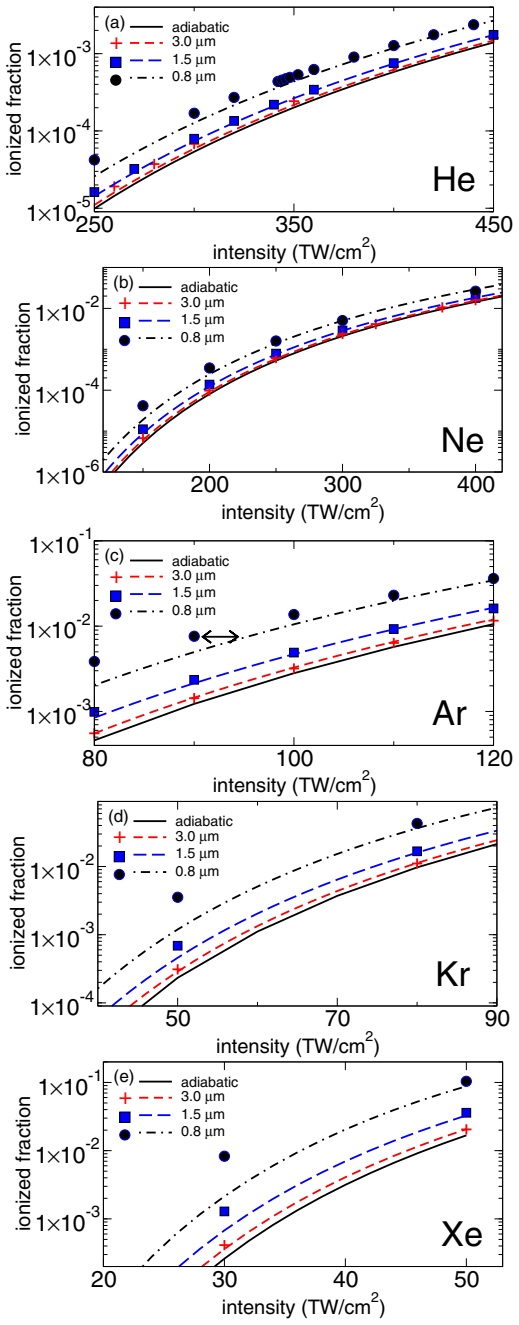

FIG. 2. Ionization fraction in noble-gas atoms exposed to excitation by a 40-fs-duration pulse with different central wavelengths of 0.8, 1.5, and 3.0 μm (shown as, from top to bottom: black, blue, and red lines and symbols). Solid lines correspond to the uncorrected single-state MESA, dashed lines show results with included post-adiabatic corrections, and symbols show TDSE simulation results.

to the precise value of E_{eff}; rather, it should be regarded as a fitting parameter for an effective model born out of a sequence of approximations. In particular, the assumption that the memory function exhibits a simple exponential decay with the time delay may be an oversimplification. Nevertheless, it is shown next that the results obtained with this model are very encouraging.

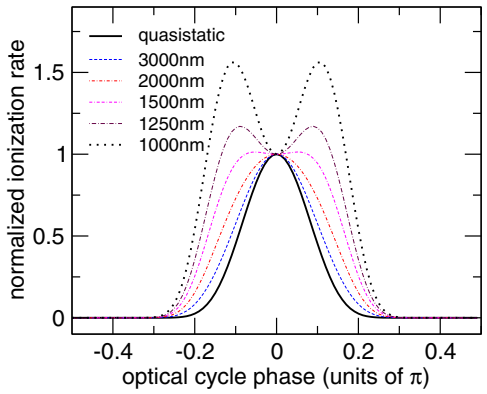

FIG. 3. The effect of the post-adiabatic correction on the ionization yield, within one half-cycle of the field with an amplitude of 0.05 a.u, for argon. The different curves are obtained with shorter excitation wavelengths and the solid black line represents the adiabatic approximation. The way the ionization is enhanced during times of fastest change of the driving field is very similar to the behavior in the post-adiabatic tunneling model of Ref. [26].

Previous results with simplified and exactly solvable models [5] suggest that the post-adiabatic correction should significantly reduce the gap between the MESA-based ionization yield and its counterpart obtained from the TDSE simulations. This is indeed what Fig. 2 shows, here for more realistic model atoms. At longer wavelengths, the correction essentially captures the target ionization yield, and at shorter wavelength it improves the result significantly. The comparison of our results for different species indicates that the correction works more accurately in lighter atoms. Also, the relative accuracy improves at higher intensities of the excitation pulse.

In the simulation of optical filamentation, which is the main intended application of the MESA, the interplay between the nonlinearity and pulse propagation effects leads to the well-known intensity clamping [25]. This suggests that one way to judge the accuracy of the post-adiabatically corrected MESA is to examine the difference in the clamped intensity inside a filament. We will look closer at this issue in the following section, but a rough answer can be seen in Fig. 2; it is the horizontal distance between a symbol and the MESA curve corresponding to the given wavelength [indicated by an arrow in Fig. 2(c)]. This suggests that in the near-infrared (NIR) region around 800 nm wavelength, the error should be twenty to thirty percent, and the accuracy further improves with increasing wavelength.

It may also be useful to visualize how and *when during the cycle* the post-adiabatic correction increases the ionization rate. The enhancement is illustrated as a function of the phase within an optical cycle in Fig. 3, which shows the ionization rate normalized to the maximum rate in Ar, driven by an oscillatory field with the amplitude of $F_0 = 0.05$ a.u. The depicted behavior is very similar to that obtained for a nonadiabatic tunnel ionization model (cf. Fig. 2 in Ref. [26]), with the yield increasing most when the field changes fastest. The figure also makes it evident that the magnitude of the correction grows quickly with decreasing wavelength.

B. Ionization in two-color pulses

For an additional test, we next investigate the ionization yield in two-color pulses. The following illustration is motivated by the recently proposed subcycle engineering of optical filaments [27–29] which uses a fundamental "pump" augmented by a weak third-harmonic seed pulse. By controlling the relative phase between the pump and the third-harmonic seed, the ionization yield can be significantly enhanced. This behavior is already qualitatively captured by the MESA in its adiabatic limit, i.e., when using a single resonant state. We shall show that the inclusion of post-adiabatic corrections can further improve the accuracy.

Figure 4 shows a comparison between the corrected MESA and TDSE simulations of ionization yields in an argon atom exposed to two-color pulses. The 35 fs waveform consists of a strong fundamental with central wavelengths of $\lambda_p = 3, 2.4, 1.5,$ and $0.8\ \mu$m (panels from top to bottom), and a weak seed at $\lambda_s = \lambda_p/3$. As the relative phase of the third harmonic pulse is varied between $\phi = 0$ and $\phi = \pi$ (depicted as curves from top down), the resulting ionization yield can change significantly, even for seed pulses that are very weak. In the present illustration we have used the seed to pump an energy fraction of 15% or 1% as indicated in the figure. The reason a smaller seed energy is used with the 800 nm pump is that for higher seed energies the ionization becomes dominated by the 266 nm wavelength, and the ionization fraction increases to tens of percent which is too far beyond the values typical for optical filamentation. These simulations were executed for argon and included the post-adiabatic correction with $E_{\text{eff}} = 0.12$. The corresponding TDSE results are depicted as symbols for select pump-pulse intensities.

It is evident from the top panel in Fig. 4 that the agreement between the MESA approximation and the TDSE "target" solution(s) is excellent at $\lambda_p = 3\ \mu$m. The orange dotted lines, only included for $\phi = \pi$ for a better readability, indicate the uncorrected yields. As one can see, while the post-adiabatic correction is relatively small, as expected for longer wavelengths, its inclusion makes the model quantitatively accurate.

The accuracy remains very good for $\lambda_p = 2.4\ \mu$m and $\lambda_p = 1.5\ \mu$m (middle panels), with the corrections being more important as the fundamental wavelength decreases. Note that, in these cases, the third harmonic is already close to the edge or inside of the visible region and, at least for the high-frequency component, one should not expect MESA to be very accurate. Yet, the post-adiabatic corrections eliminate most of the gap between the target solutions and the uncorrected, single-state MESA result.

Finally, for $\lambda_p = 0.8\ \mu$m (bottom panel) the agreement deteriorates. Here we are approaching the short-wavelength end of the MESA's applicability domain. Nevertheless, the post-adiabatic correction clearly improves the outcome, and the model ionization dynamics are still qualitatively correct, exhibiting a deep periodic dependence of the ionization rate on the seed pulse phase. (Similar to the previous example, the expected error in a pulse propagation simulation would show up as an increase in the achieved light intensity by a factor of about 30%.)

To conclude this section, our comparison with the numerically exact results for the very same model(s) used to obtain the data sets that support the MESA model show that the inclusion of the post-adiabatic corrections going beyond the single-state approach represents a computationally inexpensive way to both improve the accuracy and widen the applicability of the method. This is a significant step up from the conventional model, especially for the excitation waveforms that cannot be characterized as single color.

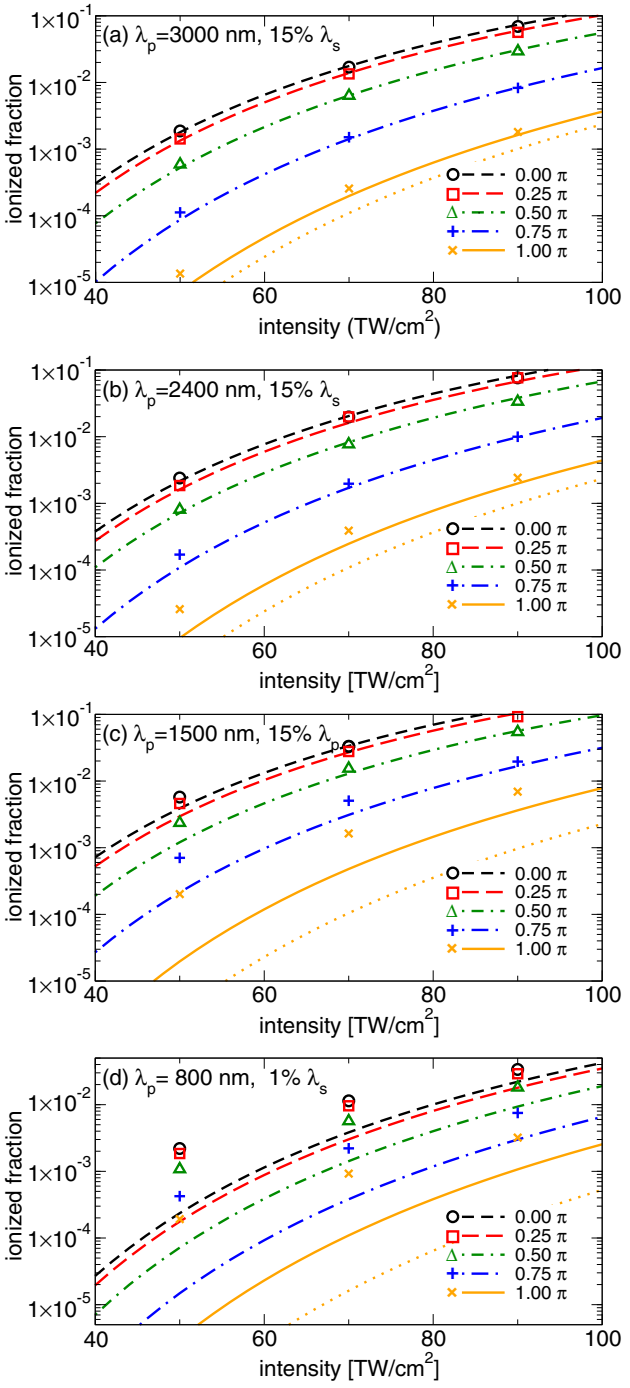

FIG. 4. Ionization yield in a two-color pulse. The relative phase ϕ between the pump and its third-harmonic seed carrying 15% or 1% of the energy can be used to control the achieved ionization levels. The MESA model results (lines) are compared to the TDSE simulations shown as symbols.

V. SIMULATION OF OPTICAL FILAMENTS

The metastable electronic state approach was designed for numerical simulation of light-matter interactions where atomic gases are exposed to different excitation fields at different locations, for which the optical filamentation is a prime example. In this section, we demonstrate that the MESA as described above can be used for the simulation of optical filamentation in noble gases across the wavelength region ranging from the near-infrared (NIR) to midinfrared (MIR). Furthermore, we compare the simulations with and without the inclusion of the post-adiabatic corrections. This gives us information about how important the corrections are at different wavelengths. Specifically, we simulate the optical filamentation at 800 nm and 2.4 μm wavelengths. The former represents a regime where MESA provides only a qualitative picture, while the latter is where it is in fact most suitable and a preferred alternative to the conventional filamentation model.

We choose to simulate a single filament with a modest pulse energy, so that we can explore a regime which is now or will soon be accessible to the experiments in the MIR range. All simulations employed a Gaussian pulse with 40 fs duration, and the peak intensity was adjusted such that the maximal power corresponding to $3P_c$ for pulses with $\lambda = 800$ nm and to $2P_c$ for $\lambda = 2.4$ μm, where the critical power for self-focusing was calculated from the nonlinear index values taken from Ref. [30].

In all cases except He and Ne, the assumed gas pressure is equal to 1 atm. For He and Ne, we increased the pressure to 10 atm. This better corresponds to the conditions that are likely to be employed in, for example, high-harmonic generation experiments [31]. Additionally, it makes it possible to observe the filamentation with a pulse energy that is more realistic from the standpoint of what sources are currently available.

In all cases, the initial beam of 3 mm $1/e^2$ radius was focused with an $f = 2$ m lens. This geometry was chosen deliberately because, in general, the dynamics in the midinfrared optical filaments are different from those at 800 nm [32]. The focused beam geometry increases the intensity reached with the MIR pulses, and thus allows us to study them in the regime in which the post-adiabatic corrections play a more important role than they otherwise would in a loosely focused beams.

We have used the GUPPECORE [33,34] simulator with a light-matter interaction plugin which implements the MESA framework as outlined in previous sections, and which utilized the data set included in the Supplemental Material [22]. The linear medium properties were described in terms of tabulated frequency-dependent susceptibility based on Sellmeier formulas taken from Ref. [35] (and from *refractiveindex.info* for Ne).

The simulation results are summarized in Fig. 5. For each simulation run, we have evaluated the expected self-focusing collapse distance using the nonlinear index from Ref. [30]. Since the n_2 values have been shown to be essentially independent of wavelength between the NIR and MIR regions [36], the expected collapse distance, shown by a dashed vertical line in the figure, provides a useful test. We have previously evaluated the nonlinear index within the MESA and found it to be in the expected range for different gases [6]. Here we can see that this alternative and perhaps more practical measure

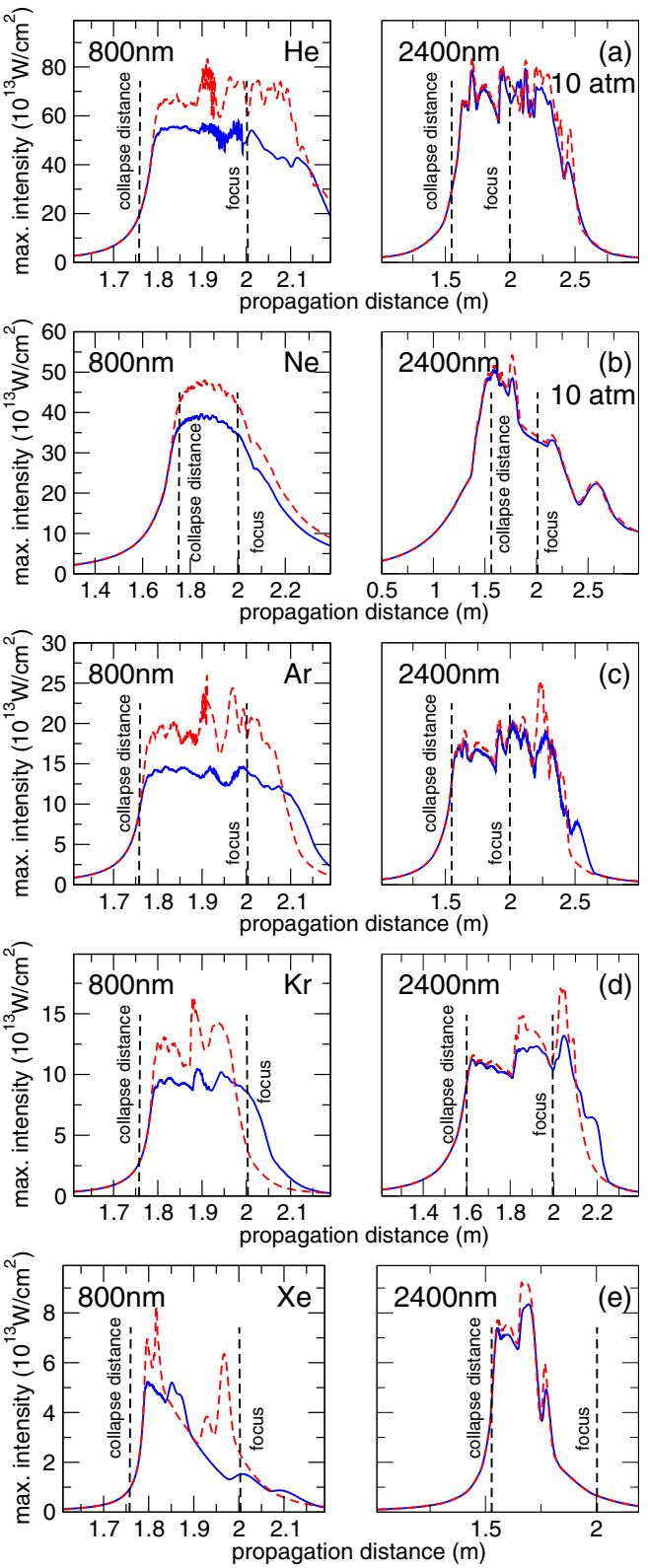

FIG. 5. Optical filament simulation using MESA based light-matter interaction model. Full lines represent the results obtained with a full model, while the dashed lines are for simulations without the post-adiabatic corrections. The vertical lines mark the position of the linear focus, and the expected self-focusing collapse distance obtained from the experimental values of the nonlinear index [30].

of nonlinearity offered by the collapse distance is also well reproduced by our models.

The comparative simulations for different central wavelengths elucidate the role the post-adiabatic corrections play in the filamentation modeling. First, for $\lambda = 800$ nm, i.e., at the edge of the applicable region of the present light-matter interaction framework, one can see that without the correction included, the resulting maximal intensity is overshot by about 20%–30%, in agreement with the estimate based on the data in Fig. 2(c). Otherwise the overall filament properties, such as length, and differences in the behavior found in different gases are qualitatively unchanged. We take this as an indication that even for this shorter wavelength, our approach provides a viable and more robust alternative to the conventional model used in optical filamentation.

At the longer wavelength, the MESA becomes more accurate, even without including the post-adiabatic correction. This is evident from the simulation data which shows that the maximal intensity is quite close with and without the corrections. In fact, throughout the leading portion of the filament they are extremely close, again in agreement with what Fig. 2(c) also suggests. At later times or at longer propagation distances we do see that the uncorrected results exhibit intensity spikes that are damped in the full model. This is especially evident in case of Ar and Kr, while the effect is much less pronounced in He, Xe and is especially weak in Ne. The behavior can be related to the supercontinuum (data not shown) generated in the filament.

The fact that the post-adiabatic corrections can sometimes show up even in longer-wavelength optical filaments is an interesting observation which shows that the midinfrared filaments are specific in what role is played by the high-frequency portion of their spectrum. Here we have evidence that the supercontinuum actually contributes to the ionization in a way that manifests as a slightly lower clamped intensity in the filament. This observation is in line with the ideas put forward in Ref. [29]. We can see that the impact of the secondary radiation becomes more important for MIR pulses. This is because, in general, in the MIR wavelength range the interplay between the nonlinearity and chromatic dispersion will almost always produce broadband spectra in which the harmonic components are a couple of orders of magnitude weaker than the fundamental. As the high-frequency components are often localized on axis, they can significantly contribute to the strong-field ionization, which in turn affects the whole pulse propagation.

VI. SUMMARY AND CONCLUSIONS

In summary, this paper has provided the theoretical background and data sets necessary to implement MESA for modeling the nonlinear optical response and strong-field ionization for a variety of noble gases. In particular, single-active-electron models were employed for He, Ne, Ar, Kr, and Xe atoms to tabulate the nonlinear dipole moment and ionization rate as functions of the applied external field. These MESA data sets have been incorporated into a nonlinear light-matter interaction module for unidirectional pulse propagation simulations, both in the adiabatic approximation and beyond. Simulations involving excitation pulses at different center wavelengths as well as ionization in two-color pulses were presented and the MESA results were found to compare well with numerical solutions of the time-dependent Schrödinger equation. Illustrative examples of the numerical simulation of high-power pulse propagation incorporating MESA data were presented and showcase the successful application to optical filamentation in the MIR region.

A general finding of this study is that MESA is most appropriate in the MIR regime, where the optical field time dependence can be considered slow in comparison to atomic timescales. To relax this assumption at shorter wavelengths higher-order metastable states were included, thereby accounting for post-adiabatic effects and associated inertial component of the nonlinear optical response. Here we approximately incorporated these higher-order states by assuming a completeness relation, thus allowing us to express the post-adiabatic corrections in terms of the lowest state. The post adiabatic corrections were validated in the NIR to MIR regions by comparing the predicted ionization rates against the TDSE solutions, the accuracy increasing with wavelength. With reference to the pulse propagation simulations in Fig. 5 for 800 nm (left column), it must be remarked that the single-state MESA predictions already provide an excellent qualitative picture, within 20%–30% of the corrected results. Since the single-state MESA is no more computationally intensive than the standard filamentation model, it provides a physically superior approach given its microscopic foundation.

Our comparative pulse propagation simulations revealed an interesting effect that deserves mention: The secondary radiation generated for a MIR optical filament can be strong enough to affect the overall ionization rate, which in turn can significantly modify the filament propagation characteristics. This is in contrast to the physical picture in the 800 nm and visible regions for which the secondary radiation may be treated as weak, and well described within a first Born approximation [37], so that feedback onto the filament propagation characteristics is weak. A detailed examination of these effects in the MIR will be the subject of a future paper.

Finally, while our main goal was to demonstrate the utility of MESA as a simulation tool, our results point to new avenues for future research. In particular, our study shows that while the post-adiabatic corrections are non-negligible they are also not overwhelming, so it is reasonable to expect that the TDSE simulations could be used to quantify and parametrize the dependence on the history of the system directly. This could help to eliminate or reduce the sequence of approximations needed in our derivations. Furthermore, the qualitative similarities between the parametrized nonlinear optical response for the variety of noble gas atoms considered strongly suggests the possibility that all MESA-related quantities could be obtained from experiments. Measurements could be used to accurately calibrate the scales of the precalculated, model-based MESA responses, while taking advantage of the fact that MESA describes both nonlinearity and ionization within a single framework.

ACKNOWLEDGMENTS

This material is based upon work supported by the Air Force Office of Scientific Research under award number FA9550-16-1-0121 (M.K.) and FA9550-13-1-0228 (A.B.).

[1] E. Lorin, M. Lytova, A. Memarian, and A. D. Bandrauk, J. Phys. A: Math. Theor. **48**, 105201 (2015).

[2] E. Lorin, S. Chelkowski, E. Zaoui, and A. Bandrauk, Phys. D **241**, 1059 (2012).

[3] M. Richter, S. Patchkovskii, F. Morales, O. Smirnova, and M. Ivanov, New J. Phys. **15**, 083012 (2013).

[4] M. Hofmann and C. Brée, Phys. Rev. A **92**, 013813 (2015).

[5] M. Kolesik, J. M. Brown, A. Teleki, P. Jakobsen, J. V. Moloney, and E. M. Wright, Optica **1**, 323 (2014).

[6] A. Bahl, J. M. Brown, E. M. Wright, and M. Kolesik, Opt. Lett. **40**, 4987 (2015).

[7] J. Brown, C. Shanor, E. Wright, and M. Kolesik, Opt. Lett. **41**, 859 (2016).

[8] A. H. Larsen, U. De Giovannini, D. L. Whitenack, A. Wasserman, and A. Rubio, J. Phys. Chem. Lett. **4**, 2734 (2013).

[9] D. Dimitrovski, C. P. J. Martiny, and L. B. Madsen, Phys. Rev. A **82**, 053404 (2010).

[10] E. Hasović, M. Busuladžić, W. Becker, and D. B. Milošević, Phys. Rev. A **84**, 063418 (2011).

[11] N. Moiseyev, Phys. Rep. **302**, 212 (1998).

[12] N. Moiseyev, *Non-Hermitian Quantum Mechanics* (Cambridge University Press, Cambridge, UK, 2011).

[13] J. M. Brown and M. Kolesik, Adv. Math. Phys. **2015**, 125832 (2015).

[14] G. García-Calderón, A. Máttar, and J. Villavicencio, Phys. Scr. **2012**, 014076 (2012).

[15] J. Brown, P. Jakobsen, A. Bahl, J. V. Moloney, and M. Kolesik, J. Math. Phys. **57**, 032105 (2016).

[16] P. T. Leung, S. Y. Liu, and K. Young, Phys. Rev. A **49**, 3982 (1994).

[17] P. T. Leung, S. Y. Liu, and K. Young, Phys. Rev. A **49**, 3057 (1994).

[18] X. M. Tong and C. D. Lin, J. Phys. B: At., Mol. Opt. Phys. **38**, 2593 (2005).

[19] F. Cloux, B. Fabre, and B. Pons, Phys. Rev. A **91**, 023415 (2015).

[20] S.-F. Zhao, L. Liu, and X.-X. Zhou, Opt. Commun. **313**, 74 (2014).

[21] E. Polizzi, Phys. Rev. B **79**, 115112 (2009).

[22] See Supplemental Material at http://link.aps.org/supplemental/10.1103/PhysRevA.94.023850 to employ the ssMESA (single state metastable electronic state approach) framework for noble gas, light-matter interaction.

[23] E. E. Serebryannikov and A. M. Zheltikov, Phys. Rev. Lett. **116**, 123901 (2016).

[24] A. Bahl, A. Teleki, P. K. Jakobsen, E. M. Wright, and M. Kolesik, J. Lightwave Technol. **32**, 3670 (2014).

[25] S. L. Chin, T.-J. Wang, C. Marceau, J. Wu, J. S. Liu, O. Kosareva, N. Panov, Y. P. Chen, J.-F. Daigle, S. Yuan, A. Azarm, W. W. Liu, T. Seideman, H. P. Zeng, M. Richardson, R. Li, and Z. Z. Xu, Laser Phys. **22**, 1 (2012).

[26] G. L. Yudin and M. Y. Ivanov, Phys. Rev. A **64**, 013409 (2001).

[27] J. Doussot, P. Béjot, G. Karras, F. Billard, and O. Faucher, J. Phys. B: At., Mol. Opt. Phys. **48**, 184005 (2015).

[28] P. Béjot, G. Karras, F. Billard, J. Doussot, E. Hertz, B. Lavorel, and O. Faucher, Phys. Rev. A **92**, 053417 (2015).

[29] P. Béjot, G. Karras, F. Billard, E. Hertz, B. Lavorel, E. Cormier, and O. Faucher, Phys. Rev. Lett. **112**, 203902 (2014).

[30] J. K. Wahlstrand, Y.-H. Cheng, and H. M. Milchberg, Phys. Rev. Lett. **109**, 113904 (2012).

[31] T. Popmintchev, M.-C. Chen, D. Popmintchev, P. Arpin, S. Brown, S. Ališauskas, G. Andriukaitis, T. Balčiunas, O. D. Mücke, A. Pugzyls, A. Baltuška, B. Shim, S. E. Schrauth, A. Gaeta, C. Hernández-García, L. Plaja, A. Becker, A. Jaron-Becker, M. M. Murnane, and H. C. Kapteyn, Science **336**, 1287 (2012).

[32] P. Panagiotopoulos, P. Whalen, M. Kolesik, and J. V. Moloney, J. Opt. Soc. Am. B **32**, 1718 (2015).

[33] M. Kolesik and J. V. Moloney, Phys. Rev. E **70**, 036604 (2004).

[34] J. Andreasen and M. Kolesik, Phys. Rev. E **86**, 036706 (2012).

[35] A. Bideau-Mehu, Y. Guern, R. Abjean, and A. Johannin-Gilles, J. Quant. Spectrosc. Radiat. Transfer **25**, 395 (1981).

[36] S. Zahedpour, J. K. Wahlstrand, and H. M. Milchberg, Opt. Lett. **40**, 5794 (2015).

[37] M. Kolesik and J. V. Moloney, Opt. Express **16**, 2971 (2008).